A competing hydrophobic tug on L596 to the membrane core unlatches S4–S5 linker elbow from TRP helix and allows TRPV4 channel to open

Jinfeng Teng[a,b], Stephen H. Loukin[a], Andriy Anishkin[c], and Ching Kung[a,d,1]

[a]Laboratory of Molecular and Cell Biology, University of Wisconsin, Madison, WI 53706; [b]Department of Physiology, University of Texas Southwestern Medical Center, Dallas, TX 75390; [c]Department of Biology, University of Maryland, College Park, MD 20742; and [d]Department of Genetics, University of Wisconsin, Madison, WI 53706

Contributed by Ching Kung, August 19, 2016 (sent for review August 28, 2015; reviewed by Ian R. Booth, Irene Iscla, and Boris Martinac)

We have some generalized physical understanding of how ion channels interact with surrounding lipids but few detailed descriptions on how interactions of particular amino acids with contacting lipids may regulate gating. Here we discovered a structure-specific interaction between an amino acid and inner-leaflet lipid that governs the gating transformations of TRPV4 (transient receptor potential vanilloid type 4). Many cation channels use a S4–S5 linker to transmit stimuli to the gate. At the start of TRPV4's linker helix is leucine 596. A hydrogen bond between the indole of W733 of the TRP helix and the backbone oxygen of L596 secures the helix/linker contact, which acts as a latch maintaining channel closure. The modeled side chain of L596 interacts with the inner lipid leaflet near the polar–nonpolar interface in our model—an interaction that we explored by mutagenesis. We examined the outward currents of TRPV4-expressing *Xenopus* oocyte upon depolarizations as well as phenotypes of expressing yeast cells. Making this residue less hydrophobic (L596A/G/W/Q/K) reduces open probability [Po; loss-of-function (LOF)], likely due to altered interactions at the polar–nonpolar interface. L596I raises Po [gain-of-function (GOF)], apparently by placing its methyl group further inward and receiving stronger water repulsion. Molecular dynamics simulations showed that the distance between the levels of α-carbons of H-bonded residues L596 and W733 is shortened in the LOFs and lengthened in the GOFs, strengthening or weakening the linker/TRP helix latch, respectively. These results highlight that L596 lipid attraction counteracts the latch bond in a tug-of-war to tune the Po of TRPV4.

TRP channels | TRP domain | gating | opening mechanism | lipids

Integral membrane proteins comprise about a quarter of the human proteome (1), and include sensors such as G protein-coupled receptors and ion channels, which are major drug targets. Conformational changes crucial to their functions—for example, channel gating—entail intimate interactions with nearby lipids. We mostly have generalized descriptions of protein–bilayer energetics and mechanics during gating, because knowledge of specific interactions is just emerging (2–4). Take the case of the most well-studied ion channel family: the voltage-gated K^+ channels (K_v). Surrounding lipids cocrystallized with K_v approximate a bilayer structure (5), and as estimated, in the budget of free-energy change during K_v gating the portion associated with the deformation of the surrounding lipid bilayer is comparable to the voltage-dependent portion (6). Though K_v is best known for its voltage sensitivity, it is in fact also highly sensitive to the bilayer stretch; its open probability can be increased by 50% by a small membrane-tension increase of only ∼1.6 mN/m (7, 8).

The present study is not primarily about the physics of mechanosensitivity, but the basic question of whether and how any localized protein–lipid interactions affect the key chemical bonds that control gating. One such bond was found in TRPV4 (transient receptor potential vanilloid type 4). In a homology model of TRPV4 based on the cryo-EM structure of TRPV1 (9, 10), L596 at the start of the S4–S5 linker helix forms a bond with W733 near the middle of the TRP helix. Not seen in K_v, this amphipathic TRP helix trails S6 and lies at the interface level of bilayer's inner leaflet but not in contact with it. Note that this hydrogen bond is between a proton in the W733's indole ring and the backbone oxygen, not the side chain, of L596. L596P, which twists the backbone, is among the over 50 mutant alleles causing blockages of bone development in human (11). Like other such human skeletal dysplasia mutations, L596P is a gain-of-function (GOF) allele, which increases open probability (Po) and causes pathologies presumably due to leakage (12). W733R mutants, selected by forward genetics based on toxicity in budding yeast (13), as well as systematically engineered W733X mutants, also increase Po, suggesting that the TRP helix contact with S4–S5 linker is secured by the L596–W733 H-bond and is used as a latch to keep the channel closed (14).

The S4–S5 linker is best known for its role in the electromechanical coupling between the periphery and the pore to control the S6 gate of K_v (15), and has been recently implicated in transduction of allosteric signals from lipids and ligands in TRPV1 channel (16). In our TRPV4 model, this S4–S5 linker begins at a sharp elbow connecting it to S4 (Fig. 1*C*). This elbow comprises four residues (G595, L596, K597, L598) exposed to lipids in a bay between the peripheral domains of neighboring subunits (Fig. 1*A*, arrow). Though the latch bond is between the invariant tryptophan W733 and the carbonyl oxygen of L596, L596's isobutyl side chain faces outward and contacts the polar–nonpolar interface of the inner-leaflet lipids (Fig. 1*C*) (14). A

Significance

Approximately 25% of the human proteome is integral membrane proteins, comprising most drug targets; these include ion channels, which change shape to open and close. There are some general descriptions on the role of surrounding lipids in such shape change, but few specifics. We have previously shown that a channel (TRPV4) uses hydrogen bonding between specific residues on the TRP helix and S4–S5 linker elbow as a latch enforcing closure. Here, by using mutations, *Xenopus* oocyte electrophysiology, budding-yeast phenotypes, and molecular simulations, we discovered that the side chain of one of the partner amino acids binds lipids at the inner polar–nonpolar interface and that this binding counteracts the hydrogen bonds, thus helping to unlatch and open the channel.

Author contributions: J.T. and C.K. designed research; J.T., S.H.L., and A.A. performed research; S.H.L. and A.A. contributed new reagents/analytic tools; J.T., S.H.L., A.A., and C.K. analyzed data; and J.T., S.H.L., A.A., and C.K. wrote the paper.

Reviewers: I.R.B., University of Aberdeen; I.I., University of Texas Southwestern Medical Center; and B.M., Victor Chang Cardiac Research Institute.

The authors declare no conflict of interest.

[1]To whom correspondence should be addressed. Email: ckung@wisc.edu.

This article contains supporting information online at www.pnas.org/lookup/suppl/doi:10.1073/pnas.1613523113/-/DCSupplemental.

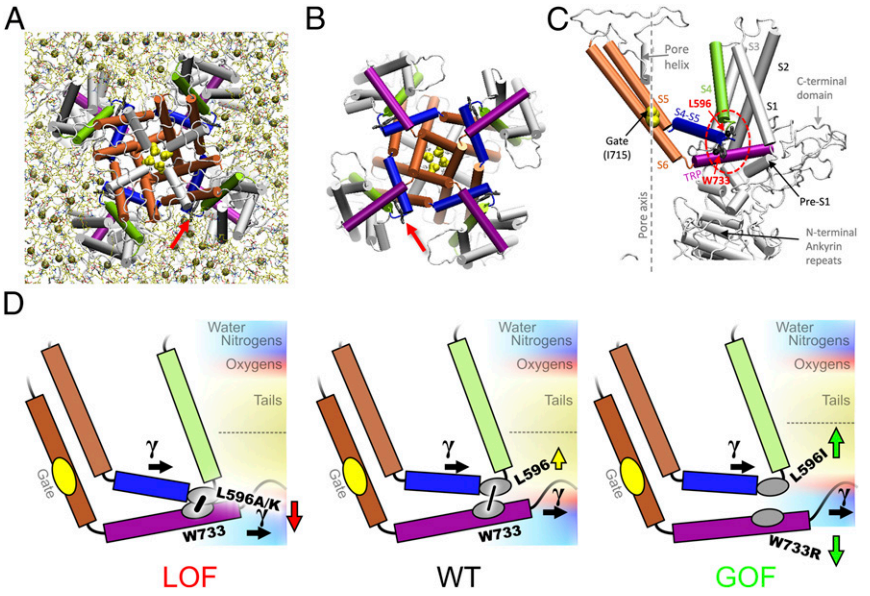

Fig. 1. Structural elements and the tug-of-war model of TRPV4 gating. A snapshot of the refined TRPV4 homology model (14), viewed from the filter (*A*) or gate (*B*) side (cytoplasmic domains not shown). Arrow marks the TRP helix/S4–S5 linker bond. There are about four lipids (tan spheres, phosphorus atoms) per bay in the inner leaflet. (*C*) In the TRPV4 subunit, S4 (green) is connected to the S4–S5 linker helix (blue) at a sharp elbow contacting the TRP helix (purple). See interactions with lipids in Fig. 5. (*D*) The expected effect of mutations based on the hydrophobicity of the introduced residue vs. the neighborhood. Mutations at L596 less hydrophobic than leucine are likely to move toward polar regions of the membrane, thus tightening the latch S4–S5 linker/TRP helix contact (low-Po LOF phenotype) (*Left*), whereas the more hydrophobic isoleucine would be pushed stronger into bilayer core, loosening the latch (GOF phenotype) (*Right*) and allowing lateral tension (γ) to open the channel. A similar unlatching effect could be caused by the pull on the TRP helix toward the polar region by charged substitutions at W733 (e.g., W733R).

hydrophobic residue (L or F) at the beginning of the linker is highly conserved in the TRPV family (14). We examined the role of this contact by analyzing the effects of amino acid substitutions at position 596 on TRPV4 gating. These effects are best explained by a balance between the side chain–membrane interaction and the bond between TRP helix and S4–S5 linker elbow, as if in a tug-of-war (Fig. 1*D*). Molecular dynamics (MD) simulations supported this model, showing that the contact between S4–S5 linker and TRP helix, represented by the distance between the levels of α-carbons of the latch-bond partners, varies systematically with the side chain–lipid interaction.

Results

L596A, W, G, Q, or K Reduces, Whereas L596I Increases, the TRPV4 Current. TRPV4 passes a nonspecific cation current that rectifies outwardly. At 3–4 d after the injection of 5 ng WT TRPV4 cRNA into *Xenopus* oocytes, ∼5 μA steady-state currents can be registered upon a step depolarization from −60 to 60 mV with a two-electrode voltage clamp (14) (Fig. 2*A*; $n > 50$). Oocytes with the same injection and incubation of mutant cRNAs were examined. L596A, W, G, Q, and K cRNAs each produced little or no steady-state currents above background (Fig. 2 *F–J*; $n > 5$ each). This lack of current was due to very low Po on depolarization, and not a lack of protein expression. Adding the strong TRPV4-specific agonist GSK 1016790A (GSK) to the bath activated huge currents, often beyond the capacity of our recording system (Fig. 2*K* and Fig. S1; $n > 3$ each). We refer to these channels with low Po's as loss-of function (LOF) mutant channels. L596V or L596F cRNA produced currents not significantly different from those of the WT (Fig. 2 *D* and *E*; $n > 15$ each). Surprisingly, cRNA of L596I, with only an isomerized isobutyl side chain, produced very large currents and appeared to be unusually toxic to oocytes. We lowered the amount of injected cRNA to 1 ng and registered large L596I currents (Fig. 2*C*; $n > 50$), comparable to those of WT at 5 ng injection. The size of L596I current is reminiscent of those of W733X and L596P, which apparently weaken the W–L hydrogen bond (14). W733Q currents (at 0.1 ng cRNA; $n > 5$) are shown in Fig. 2*B* for comparison. We call channels with increased Po GOF mutant channels.

Activation and Inactivation. Prominent activation of the WT TRPV4 is evident at 60 mV with outward current peaking at ∼70 ms followed by current decline due to inactivation (13) (Fig. 3*A*, black arrow). At 40 mV, the feeble activation is immediately followed by inactivation (τ ∼95 ms; Fig. 3*A*, red arrow). Though there were few discernable currents from the LOF mutants in our usual procedures (Fig. 2 *F–J*), measurable currents could often be seen after injecting increased amount of cRNA (10–25 ng). For example, L596A trajectory of the outward current at 60 mV resembled that of the WT at 40 mV (Fig. 3*B*, red arrow; inactivation τ ∼83 ms, $n = 8$). Even at 100 mV, WT-like activation was not observed. Massive injection of cRNA, however, could often compromise the health of the oocytes, causing larger leak current and complicating interpretation. We have therefore contrived a L596A E797K double mutant harboring a second mutation in the cytoplasmic domain that boosts the basal Po (17). Though the E797K channel had current activation and inactivation kinetics typical of GOF mutants (17), the double mutant (standard 5-ng injection) again only showed the decaying outward current even upon strong depolarizations (Fig. 3*C*, red arrow; two-phased inactivation τ_1 ∼9 ms, τ_2 ∼94 ms, $n = 10$). These findings indicate that the LOF channels could not be fully activated, and strongly favor the impermeable states (closed or inactivated). The kinetics of the outward currents from conservative mutant L596F resembled those of the WT. Stepping to 60 mV, the WT (Fig. 3*D*; $n = 11$) and L596F channel (Fig. 3*E*; $n = 4$) activated with τ_1 ∼6 ms, τ_2 ∼25 ms and inactivated in two phases (τ_1 ∼450 ms, τ_2 ∼1.6 s). The activation of the GOF L596I (at 1 ng injection; Fig. 3*F*) was similar to the WT, but its inactivation was dominated by the slow process (τ ∼1.9 s, $n = 4$). Lack of inactivation has been observed previously in TRPV4 with W733X's GOF mutations, which break the latch bond (14).

Response to GSK or Cell Swelling. TRPs are polymodal channels able to integrate disparate chemical, thermal, mechanical, and electric stimuli. To test whether L596X mutant channels are specifically deficient in their responses to depolarization, we measured their responses to the agonist GSK and to membrane stretch upon cell swelling. At 40 mV, the steady-state currents in different GSK concentrations were recorded. As shown in Fig. S2, the dose–response curve of the LOF L596A mutant channel is clearly shifted to the right compared with the WT curve. For example, at 100 nM GSK, the WT channels were strongly activated while the L596A channels were only barely activated. The GOF L596I curve appears to be left-shifted. However, the toxic effect of L596I and the added insult of >100 nM GSK likely damaged the oocytes and resulted in smaller responses (Fig. S2).

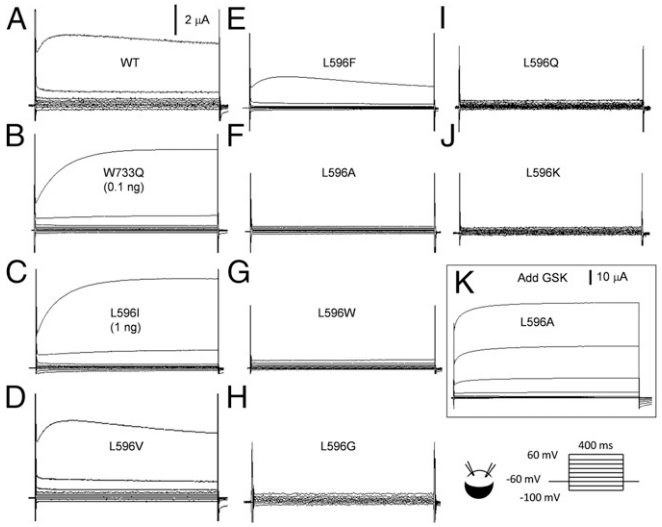

Fig. 2. Representative traces of whole-oocyte currents. Currents were recorded with a two-electrode voltage clamp from whole oocytes expressing (*A*) WT TRPV4, (*B*) GOF mutant W733Q, (*C*) GOF mutant L596I, and (*D* and *E*) the conservative mutants L596V and L596F. (*F–J*) Currents from oocytes expressing LOF TRPV4 mutant L596A, L596W, L596G, L596Q, and L596K. (*K*) L596A currents after the application of 1 μM GSK (note current scale change). All oocytes were injected with 5 ng cRNA, except those marked.

The TRPV4 gene was originally cloned based on a swelling-induced signal in expressing cells (18, 19). We tested the TRPV4 current at 60 mV during the course of oocyte swelling upon bath dilution. This current rose to a maximum over several minutes after the perfusion of a hypotonic solution in the case of the WT (12) and the conservative mutant L596F (Fig. S3 *A* and *B*). The swelling-induced current (compared with that before swelling) appeared larger in oocytes expressing the GOF mutant L596I (Fig. S3*C*). Swelling-induced current increase of those expressing the LOF mutant channels, if existed, was not obvious (Fig. S3 *E* and *F*); this could be because they are not sensitive to swelling or because their very low Po obscured even a several-fold increase. We therefore tested the L596A E797K double mutant using second mutation to magnify the basal Po (see above) (17). The L596A E797K double mutant was responsive to cell swelling (Fig. S3*G*), indicating that the LOF mutation, such as L596A, did not completely eliminate mechanosensitivity, though it responded poorly, as judged by the small proportional increase before and after swelling. The apparent stronger responses for the GOF (L596I) to ligand or swelling stimuli, the clearly feeble responses of the LOF mutant channels might indicate a central "force hub" defect and rather than deficiency in sensing a particular stimulus modality.

Yeast Phenotypes. TRPV4 has been functionally expressed in the budding yeast *Saccharomyces cerevisiae* in the membranes of an internal Ca^{2+} store (20). Ca^{2+} leakage through excessive TRPV4 activity from this store can stop yeast growth, a phenotype that has been used to select for severe GOF mutants such as W733R (13). The backbone-twisting L596P, a human mutation, also hampers yeast growth (14). Placed behind the inducible *Gal4* promoter, plasmids with the GOF W733R or L596I mutant permitted growth in a noninducing medium (glucose) but stopped growth in an inducing medium (galactose; Fig. 4*A*, second and third rows). Neither WT nor LOF channels hamper growth when expressed (Fig. 4*A*). Delivered with a second selectable plasmid, GSK inhibited the growth of cells expressing the WT TRPV4 or those with conservative mutations L596F and L596V (behind a constitutive *GPD* promoter; Fig. 4*B*, columns 2–4). The growth of cells expressing LOF mutations L596A or L596Q, however, was permitted by the delivered GSK, proving that these channels rarely opened even when heterologously expressed in vivo (Fig. 4*B*, columns 5 and 6, middle row); they nonetheless inhibited growth at high GSK concentration, showing that they were expressed and functional, albeit with lower Po's (bottom row). Cells expressing the L596I GOF TRPV4 inhibited growth even without GSK (Fig. 4*B*, rightmost column).

Molecular Dynamics Simulations. Effects of the substitutions at the position 596, as shown by oocyte electrophysiology and yeast phenotypes above, strongly correlate with the hydrophobicity of the introduced residue, for example, by hydrophobicity scales proposed in refs. 21–23. The scales, however, are only a qualitative guide, as in reality hydrophobicity also depends on microenvironment. To seek an understanding at atomic scale, we used MD simulations of TRPV4 channel model in explicit all-atom membrane/water medium to see the neighborhood of residue 596. We have previously erected a full-length homology model of a closed TRPV4, refined through MD simulation in 1-palmitoyl-2-oleoyl-phosphatidylcholine (POPC) (14). Here we explored four TRPV4 mutants based on the refined model: L596I (GOF), L596A (LOF), L596K (LOF), and W733R (GOF) (14). The simulations were not intended to reproduce the whole gating transition, which is likely much slower, but rather to visualize the environment of the "latch" residues and to reveal the initial structural changes caused by mutations underlying the phenotypes. We performed simulations and symmetry-driven structure refinement of the mutants in the same conditions as WT and compared the changes near the substituted residues. The refinement length of the WT was extended to match the mutants. The refinements have

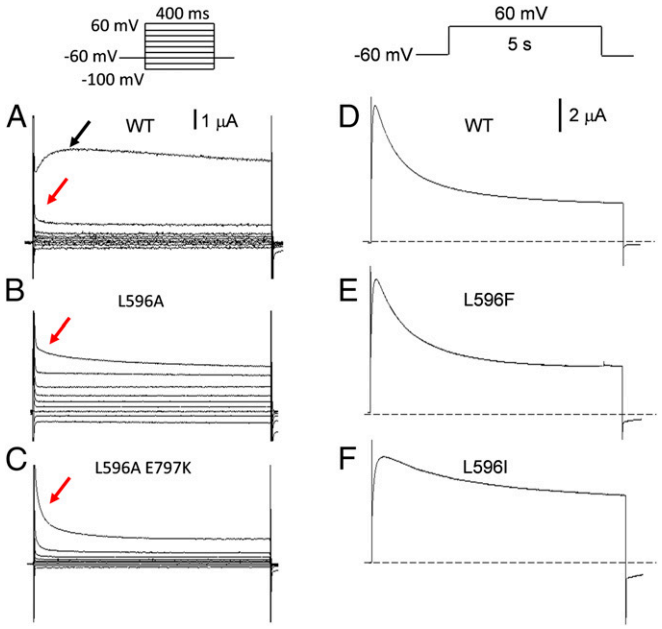

Fig. 3. Kinetics of WT and mutant TRPV4 currents. (*A*) Strong activation is evident in the WT (5-ng injection) at 60 mV (black arrow, $n > 50$), not at 40 mV (red arrow, $n = 7$). (*B*) Currents from the L596A mutant were made detectable after massive cRNA injection (15 ng). Such currents had kinetics that resembled those of the WT upon weak activation (red arrow). (*C*) The currents of the L596A E797K double mutant, with standard 5-ng cRNA injection, also showed weak activation (red arrow). E797K is used here as a background GOF mutation to boost basal Po. At a slower time base, the WT (*D*) and the conserved mutant L596F current (*E*) showed similar activation and inactivation kinetics, reaching steady state in 5 s (*F*). The GOF mutant L596I (1-ng injection) showed a slow decay even beyond 5 s.

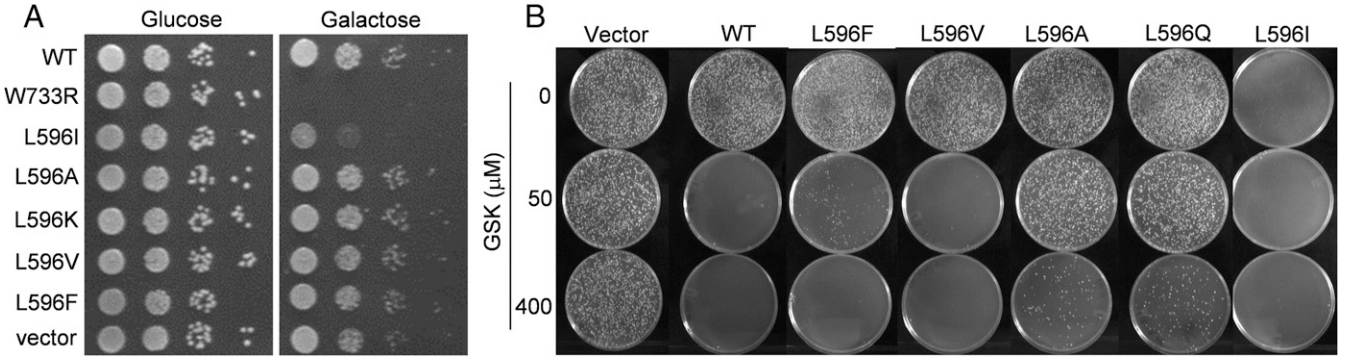

Fig. 4. Growth phenotypes of budding yeast transformed with plasmids bearing GOF or LOF mutant TRPV4. (*A*) Starting with ∼5,000 colony-forming units, serial 10-fold dilutions were dropped on plates. Placed behind an inducible promoter, plasmids with the GOF mutants W733R and L596I (second and third row) inhibited yeast growth on the inducing galactose medium (*Right*) where the channels were expressed, but not in the noninducing glucose medium (*Left*). Those with WT, conservative mutants (L596F, V) or LOF mutants (L596A, K) did not inhibit growth. Typical of three independent tests. (*B*) GSK, infiltrated into the cytoplasm during transformation, stopped the plate growth of yeast constitutively expressing plasmid with WT TRPV4 or those with the conservative mutations (L596F, L596V). Those bearing TRPV4 with LOF mutations (L596A, L596Q) grew normally at low GSK concentration, but grew slower at a higher concentration. The GOF L596I hampered growth even without GSK (only small colonies can be observed on the plates). Marked are the GSK concentrations used during transformation, not those in the cytoplasm. Typical of four independent tests.

revealed that besides bonding to L596, the side chain of W733 H-bonds to the backbone oxygen of R594. It agrees with the cryo-EM structure of another TRP homolog, TRPV2 (24) (*Discussion*). Fig. 5*A* shows that the side chain of L596 in WT reaches the hydrophobic tails of POPC, but the beginning of the side chain is at the level of glycerol oxygens and contacts the H-bonded water network (Table S1). In the direction normal to the membrane, the distance between the levels of α-carbons of L596 and W733, the two latch-bond residues, was found to be 5.9 Å (Table S2). Fig. 5*B* shows that in the L596I GOF substitution, the I596's side chain is located somewhat closer toward the bilayer core (green arrow). Compared with the leucine structure, the branching methyl in isoleucine is one carbon closer to membrane interface. It agrees with 20% higher contacts with water (Table S1), likely causing stronger hydrophobic push toward the core. Indeed, interactions with the polar lipid groups decreases, and the ratio of polar–nonpolar lipid contacts decreases by 23%; it concurs with isoleucine being more hydrophobic and suggests development of the drive toward the core, thus favoring disruption of TRP helix/S4–S5 linker elbow contact. The distance between the α-carbon levels slightly lengthened to 6.0 Å. The helix and the elbow moved away from the pore axis by 0.3 Å, consistent with facilitated gating. Simulations of W733R (Fig. 5*C*), known to be a GOF by greatly weakening the latch bond (14), show significant changes in the environment of the mutated residue. The number of waters contacting more polar arginine grows by 20%. The distance between the α-carbon levels drops to 5.6 Å; however, the electrostatic association of the 733 side chain with the backbone of L596 and R594 is disrupted, a hallmark of GOF W733X mutants. The L596 side chain acquires a less polar environment (30% lower polar–nonpolar ratio). In the case of R733, the change was caused by attraction of the arginine side chain to the oxygens of the lipid phosphates and water. In contrast to L596I, the side chains of the LOF L596A and L596K were found to be farther from the membrane core (Fig. 5 *D* and *E*, red arrows), the α-carbon distances decreased to 5.0 and 5.2 Å, respectively, and both TRP helix and S4–S5 linker elbow shifted closer to the pore axis by ∼0.3 Å. The L596A mutant has much smaller side chain, depleting polar (by 49%) and nonpolar (by 78%) contacts with lipids (137% higher polar–nonpolar ratio). The contacts with water grew by 17%; it complies with alanine being less hydrophobic and indicates loss of the attractive van der Waals interactions with the core, thus stabilizing the helix/elbow contact. The last mutant, L596K, shows very different change in contacts—positively charged lysine strongly

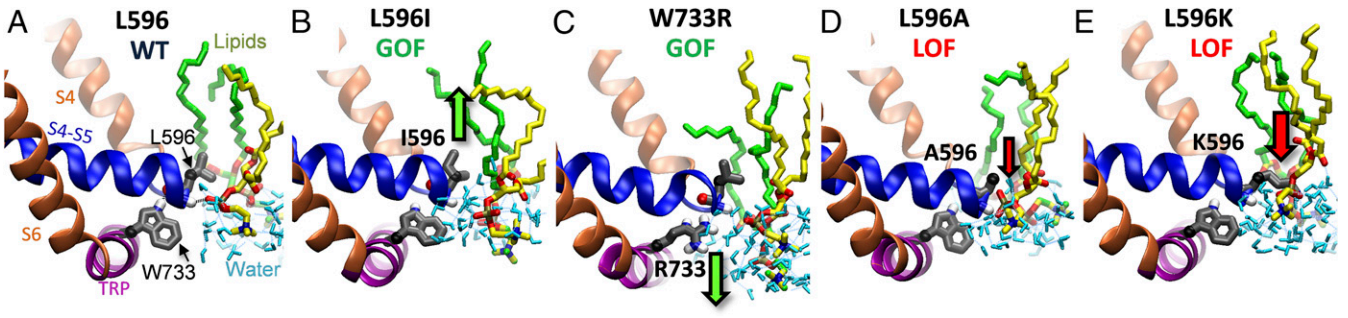

Fig. 5. Changes in protein–lipid interactions caused by mutations at W733/L596 latch. (*A*) A snapshot from molecular dynamics simulation of WT channel showing the latch bond between the indole of W733 and the backbone oxygen of L596 as well as the location of L596's isobutyl side chain contacting the lipid head group (oxygens marked red) and waters (aqua). Four presented homology models (*B*–*E*) were created by introducing mutation to the refined model of the WT channel, followed by refinement through MD simulation and symmetry-driven annealing in the explicit medium. The arrows indicate the direction of the residue displacement comparing to WT (*A*). Green arrows represent GOF mutants and where displacement favors widening the gap between S4–S5 linker and TRP helix due to (*B*) increased push toward membrane core (L596I) or (*C*) pull on TRP helix toward water and negative charges of lipids (W733R). Red arrows correspond to displacement in LOF mutants tightening S4–S5 linker/TRP helix contact caused by (*D*) decreased hydrophobic push from water (L596A) or (*E*) pull on S4–S5 linker toward lipids head groups (L596K).

engages with the lipid polar groups, especially the phosphates; because they are positioned closer to the bilayer surface, it drives K596 away from the core, thus strengthening the helix/elbow contact, matching the LOF phenotype of the mutant.

We should note that the changes in the helix/elbow forces are not confined only to a mutated side chain. As the side chain changes, its contacts with the neighboring protein groups change too. GOF mutants L596I and W733R show increased contacts of the side chain 596 with T593, L598, and T599; that shields the latter from interactions with lipids and water. In contrast, LOF L596A and L596K lower the interactions with these residues by up to 92%, thus exposing them to forces from the medium. These changes likely contribute to the push/pull balance at the latch.

Discussion

Our oocyte electrophysiological findings show that substitutions of L596 with residues that are polar or charged favor the impermeable states (closed or inactivated) and thereby greatly reduce open probability (Po). Even those that are just less hydrophobic, such as L596A, clearly reduce Po (Figs. 2 and 3). However, L596I increases Po and weakens inactivation (Figs. 2 and 3), resembling W733X or L596P mutations that weaken or break the latch bond (however, by the measures of several phenotypes, L596I is not as strong a GOF mutation as W733X) (14).

On average, valine, phenylalanine, and leucine have a very similar hydrophobicity (21–23). Phenylalanine replaces leucine in other channels of the TRPV subfamily, explaining the near-normal channel behavior of the L596V and L596F mutants. The Po and kinetic variations are consistent with the phenotypes in transgenic yeast, an entirely different in vivo system (Fig. 4). These findings indicate that the hydrophobicity of residue 596 is a key determinant of TRPV4 gating.

Structural Interpretations. Interpretations of L596X phenotypes can be based on the drive on side chain 596 toward more hydrophobic or hydrophilic environments. However, such interpretations require knowledge of the nearby atomic groups and feasibility for the residue to experience change in the external force with mutations. Hence, the MD simulations were performed (Fig. 5). The interaction between L596 side chain and its environment should create a hydrophobic force, normal to the membrane plane, driving the side chain toward the membrane core, counteracting the latch bond between W733's indole and backbone oxygens of L596 and R594 (Fig. 5*A*). L596I mutation brings the branching methyl group one carbon closer to the polar region, so water would push I596 stronger toward the membrane core. This push weakens the latch between the S4–S5 linker and TRP-helix as reflected in slight increase in the α-carbon distance of the bonding partners and outward displacement of TRP helix and S4–S5 linker elbow (Fig. 5*B* and Table S2). Destabilization of the latch contact can be achieved from the opposite side, by mutating the other partner, W733, to arginine (Fig. 5*C*), which disrupts bonding to the elbow backbone and replaces it with the pull of the TRP-helix toward water, away from the membrane core. In contrast, when applied to the opposite side of the helix–elbow contact, the weakened pull to the core inhibits TRPV4. The LOF L596A mutation significantly decreases the number of contacts, which strongly diminishes the hydrophobic force from water toward the membrane core as well as the attractive van der Waals interactions with hydrocarbon tails, as evident by the decrease in α-carbon distance strengthening S4–S5 linker/TRP helix association (Fig. 5*D*). The LOF mutation L596K has its positively charged side chain pulled to interact with negative charges of the oxygens of POPC's phosphate group, also resulted in the decrease in α-carbon distance (Fig. 5*E*). Both LOF mutations result in the helix and elbow displacement closer to the pore axis—opposite the expected gating direction. Recall that the TRP helix is directly bound to S6, and the elbow between S4 and the S4–S5 linker likely controls the S6 gate through S5/S6 helices coupling (Fig. 1 *B–D*). Thus, gating depends on the relative position of the S4–S5 linker and the TRP helix, and this position depends on a balance between the strength of the latch bond and the side chain 596-to-lipid interaction in the direction normal to the membrane. In this tug-of-war, cartooned in Fig. 1*D*, disrupting the latch is likely to facilitate the expansion of the TRP helix and the S4-to-linker elbow coupled to the gate in the lateral direction under the action of membrane tension; this is supported by the strong correlation of the outward displacement of both TRP helix and the S4-to-linker with GOF phenotype and their shift back toward the pore axis in LOF mutants as is observed in simulations (Table S2). A possible reason for this facilitation of expansion by the contact disruption is that these two domains are likely to move laterally in somewhat different directions on channel opening, because they are positioned at an angle to each other, are connected to different hinge points to other protein domains, and are receiving tension from different membrane regions. MD simulations indicate that, in the closed state, the TRP helix does not contact the lipids in the bay (Figs. 1*A* and 5*A*), but might receive tension from its C terminus protruding to the membrane. Unlike the TRP domain, the S4-to-linker elbow has direct contact with the lipids in the bay (Figs. 1*A* and 5*A*).

The S4-to-Linker Elbow. At this elbow, besides the side chain of L596, the backbone oxygen of G595, and the backbone NH of K597 and L598 (but not their side chains) also contact lipids in the bay. These contacts, as parts of a team in the tug-of-war, should also contribute to the force counteracting the latch bonds of W733 with L596 and R594. It is beyond the scope of this paper to examine all these contacts. As an example, we tested K597. K597E is clearly a LOF mutation causing a very low Po (Fig. S4). In MD simulation, our structural model has the side chain of K597 facing water and its backbone hydrogen binds to the phosphate oxygens of lipids to receive tension from lipids. K596E mutation likely causes the formation of E597–K730 salt bridge, which would add an extra tie between the TRP helix and S4–S5 linker and could turn the residue 596 around so that the backbone would lose contact with the phosphate oxygens of the lipid and restrain TRP helix in place, restricting movement under tension.

TRP Channels Are Polymodal. Here, depolarization (Figs. 2 and 3), an agonist (Fig. 2 and Fig. S2), and cell swelling (Fig. S3) are all shown to open WT TRPV4. Responses to all three stimuli are clearly weaker in the LOFs, although their being stronger in L596I (GOF) appears to be somewhat attenuated by the toxicity. In the complex environment, for the live yeast cells (presumably experiencing multiple stimuli), both the LOF and the GOF phenotypes of the TRPV4 mutants are clearly observed (Fig. 4). A parsimonious interpretation is therefore not because the sensitivities of all three sensors or receptors are coincidentally changed, but because the strength of the central latch bond systematically varies with the mutations. These results therefore indicate that all three stimuli funnel through the S4–S5 linker and/or TRP helix to mechanically open the S6 gate.

Model. Based on our findings, we envision the physiological gating of WT TRPV4 to be as follows: At rest, the tug-of-war at L596 holds the S4 linker elbow and the TRP helix in a balance that favors closure. Certain stimuli (e.g., depolarization) act on the linker, while other stimuli (e.g., Ca^{2+}-calmodulin) act on the TRP helix or on both of them (e.g., membrane stretch). These actions establish new balances in favor of opening. Topology and sequence conservation indicate important functions of the S1–S4 peripheral domain and the S4–S5 linker in TRPV channels, likely similar to those in K_v (7, 8). The TRP helix is followed by cytoplasmic domains used in Ca^{2+}-calmodulin regulation (17); it also has bonds with the pre-S1 helix and the preceding domains at the N-terminal end, and is therefore capable of receiving

cytoplasmic stimuli. The TRP helix–S4 linker elbow contact might unlatch in response to the motion of the ankyrin repeats that have been implicated in gating (10) and inactivation (24). Thus, the tug-of-war between the elbow and the TRP helix can be considered the "force hub" to integrate various stimuli, explaining polymodality. The TRP helix is not found in K_v, Ca_v, or Na_v, and may have evolved for this integration and as a safeguard to enforce closure at rest. The tug-of-war mechanism may be general to many TRP channels; this holds true in the recently published TRPV1 structure in membrane nanodiscs (16), as well as cryo-EM TRPV2 structure (24) (Fig. S5). The TRPV2 elbow, however, is one residue longer. As a result, instead of a H-bond to the backbone of F517 (homolog of L596), the tryptophan on TRP helix interacts with the backbone oxygens of Q518 and R515, structurally close to the two H-bonds to L596 and R594 oxygens in our refined TRPV4 models (Fig. S5).The tryptophan is invariant among all TRPV family members, and a TRPV3 W692G substitution here is a GOF allele causing Olmsted syndrome, a human skin disorder (25). The typical TRP-box motif is not present in TRPA family; however, TRPA1 structures have revealed a TRP-like helix in an analogous position, a proposed convergent point of allosteric chemonociception signals (26). Instead of a tryptophan/leucine couple, there is an arginine/glutamate pair capable of forming a salt bridge between the side chains.

Nonetheless, the elbow-TRP domain tug-of-war is not likely the only focus where the forces from lipid work directly, given that the inner part of S5 helix is exposed to lipids in the bay, along with the entire periphery of S1–S4 domain. Protruding into the membrane is also the C-terminal extension of the TRP helix, which can transmit the lipid forces to loosen the latch contact and facilitate opening. Not all interactions between lipids and amino acid side chains are as pivotal as that of L596, however. For example, I529 of S2 in the peripheral domain is in contact with lipids, but I529A has no discernable effects on gating (Fig. S6). A comprehensive "force roadmap" of the channel response to tension requires further exploration at the bench and in silico.

Prospective. In contrast to a general physical description of forces and energies associated with channel–lipid interaction during gating, we revealed and simulated, in atomic detail, a key focal chemical interaction between amino acids and lipids. Identifying the cruxes of specific interaction between amino acids and lipids should help fundamental understanding of other membrane proteins, be they channels, receptors, or enzymes.

Methods

Xenopus oocytes were injected with in vitro-synthesized TRPV4 cRNAs and recorded with a TEVC (two-electrode voltage clamp) after 3–4 d (14, 27). Plasmid-borne TRPV4s were expressed and growth-phenotyped in yeast (14, 28). We modeled TRPV4 in a POPC bilayer (14) using Modeler and VMD (29, 30). MD simulations were done with NAMD (31) in an all-atom medium with CHARMM36 (32, 33), force field, TIP3P water model (34), and PME electrostatics (35) with a 12-Å cutoff as an NPT ensemble in a periodic cell at 303.15 °K. We refined structures with symmetry-driven simulated annealing (36). Results were analyzed and visualized using VMD (30). See *SI Methods* for details.

ACKNOWLEDGMENTS. Support for this work was provided by NIH Grant GM096088 (to J.T., S.H.L., and C.K.); the Vilas Trust of the University of Wisconsin (J.T., S.H.L., and C.K.); and the Department of Biology, University of Maryland (A.A.).

1. Fagerberg L, Jonasson K, von Heijne G, Uhlén M, Berglund L (2010) Prediction of the human membrane proteome. *Proteomics* 10(6):1141–1149.
2. Lundbaek JA, Birn P, Girshman J, Hansen AJ, Andersen OS (1996) Membrane stiffness and channel function. *Biochemistry* 35(12):3825–3830.
3. Phillips R, Ursell T, Wiggins P, Sens P (2009) Emerging roles for lipids in shaping membrane-protein function. *Nature* 459(7245):379–385.
4. Battle AR, et al. (2015) Lipid-protein interactions: Lessons learned from stress. *Biochim Biophys Acta* 1848(9):1744–1756.
5. Long SB, Tao X, Campbell EB, MacKinnon R (2007) Atomic structure of a voltage-dependent K+ channel in a lipid membrane-like environment. *Nature* 450(7168): 376–382.
6. Reeves D, Ursell T, Sens P, Kondev J, Phillips R (2008) Membrane mechanics as a probe of ion-channel gating mechanisms. *Phys Rev E Stat Nonlin Soft Matter Phys* 78(4 Pt 1): 041901.
7. Schmidt D, MacKinnon R (2008) Voltage-dependent K+ channel gating and voltage sensor toxin sensitivity depend on the mechanical state of the lipid membrane. *Proc Natl Acad Sci USA* 105(49):19276–19281.
8. Schmidt D, del Mármol J, MacKinnon R (2012) Mechanistic basis for low threshold mechanosensitivity in voltage-dependent K+ channels. *Proc Natl Acad Sci USA* 109(26):10352–10357.
9. Liao M, Cao E, Julius D, Cheng Y (2013) Structure of the TRPV1 ion channel determined by electron cryo-microscopy. *Nature* 504(7478):107–112.
10. Cao E, Liao M, Cheng Y, Julius D (2013) TRPV1 structures in distinct conformations reveal activation mechanisms. *Nature* 504(7478):113–118.
11. Nilius B, Voets T (2013) The puzzle of TRPV4 channelopathies. *EMBO Rep* 14(2): 152–163.
12. Loukin S, Su Z, Kung C (2011) Increased basal activity is a key determinant in the severity of human skeletal dysplasia caused by TRPV4 mutations. *PLoS One* 6(5): e19533.
13. Loukin S, Su Z, Zhou X, Kung C (2010) Forward genetic analysis reveals multiple gating mechanisms of TRPV4. *J Biol Chem* 285(26):19884–19890.
14. Teng J, Loukin SH, Anishkin A, Kung C (2015) L596-W733 bond between the start of the S4-S5 linker and the TRP box stabilizes the closed state of TRPV4 channel. *Proc Natl Acad Sci USA* 112(11):3386–3391.
15. Long SB, Campbell EB, Mackinnon R (2005) Voltage sensor of Kv1.2: Structural basis of electromechanical coupling. *Science* 309(5736):903–908.
16. Gao Y, Cao E, Julius D, Cheng Y (2016) TRPV1 structures in nanodiscs reveal mechanisms of ligand and lipid action. *Nature* 534(7607):347–351.
17. Loukin SH, Teng J, Kung C (2015) A channelopathy mechanism revealed by direct calmodulin activation of TrpV4. *Proc Natl Acad Sci USA* 112(30):9400–9405.
18. Liedtke W, et al. (2000) Vanilloid receptor-related osmotically activated channel (VR-OAC), a candidate vertebrate osmoreceptor. *Cell* 103(3):525–535.
19. Strotmann R, Harteneck C, Nunnenmacher K, Schultz G, Plant TD (2000) OTRPC4, a nonselective cation channel that confers sensitivity to extracellular osmolarity. *Nat Cell Biol* 2(10):695–702.
20. Loukin SH, Su Z, Kung C (2009) Hypotonic shocks activate rat TRPV4 in yeast in the absence of polyunsaturated fatty acids. *FEBS Lett* 583(4):754–758.
21. Manavalan P, Ponnuswamy PK (1978) Hydrophobic character of amino acid residues in globular proteins. *Nature* 275(5681):673–674.
22. Kyte J, Doolittle RF (1982) A simple method for displaying the hydropathic character of a protein. *J Mol Biol* 157(1):105–132.
23. Sweet RM, Eisenberg D (1983) Correlation of sequence hydrophobicities measures similarity in three-dimensional protein structure. *J Mol Biol* 171(4):479–488.
24. Zubcevic L, et al. (2016) Cryo-electron microscopy structure of the TRPV2 ion channel. *Nat Struct Mol Biol* 23(2):180–186.
25. Lin Z, et al. (2012) Exome sequencing reveals mutations in TRPV3 as a cause of Olmsted syndrome. *Am J Hum Genet* 90(3):558–564.
26. Paulsen CE, Armache JP, Gao Y, Cheng Y, Julius D (2015) Structure of the TRPA1 ion channel suggests regulatory mechanisms. *Nature* 520(7548):511–517.
27. Teng J, Loukin S, Zhou X, Kung C (2013) Yeast luminometric and *Xenopus* oocyte electrophysiological examinations of the molecular mechanosensitivity of TRPV4. *J Vis Exp*, 10.3791/50816.
28. Loukin S, Zhou X, Su Z, Saimi Y, Kung C (2010) Wild-type and brachyolmia-causing mutant TRPV4 channels respond directly to stretch force. *J Biol Chem* 285(35): 27176–27181.
29. Eswar N, et al. (2006) Comparative protein structure modeling using Modeller. *Curr Protoc Protein Sci*, 10.1002/0471140864.
30. Humphrey W, Dalke A, Schulten K (1996) VMD: Visual molecular dynamics. *J Mol Graph* 14(1):27–38.
31. Phillips JC, et al. (2005) Scalable molecular dynamics with NAMD. *J Comput Chem* 26(16):1781–1802.
32. MacKerell AD, et al. (1998) All-atom empirical potential for molecular modeling and dynamics studies of proteins. *J Phys Chem B* 102(18):3586–3616.
33. Klauda JB, et al. (2010) Update of the CHARMM all-atom additive force field for lipids: Validation on six lipid types. *J Phys Chem B* 114(23):7830–7843.
34. Jorgensen WLCJ (1983) Comparison of simple potential functions for simulating liquid water. *J Chem Phys* 79:926–935.
35. Darden T, York D, Pedersen L (1993) Particle mesh Ewald: An N·log(N) method for Ewald sums in large systems. *J Chem Phys* 98(12):10089.
36. Anishkin A, Milac AL, Guy HR (2010) Symmetry-restrained molecular dynamics simulations improve homology models of potassium channels. *Proteins* 78(4):932–949.
37. Gietz RD, Schiestl RH (2007) Large-scale high-efficiency yeast transformation using the LiAc/SS carrier DNA/PEG method. *Nat Protoc* 2(1):38–41.
38. Rostkowski M, Olsson MH, Søndergaard CR, Jensen JH (2011) Graphical analysis of pH-dependent properties of proteins predicted using PROPKA. *BMC Struct Biol* 11:6.
39. Martyna GJTDJ, Klein ML (1994) Constant pressure molecular dynamics algorithms. *J Chem Phys* 101:4177–4189.
40. Feller SE, Zhang Y, Pastor RW, Brooks BR (1995) Constant pressure molecular dynamics simulation: The Langevin piston method. *J Chem Phys* 103(11):4613.